JCTC Journal of Chemical Theory and Computation

Article

pubs.acs.org/JCTC

Accuracy of Embedded Fragment Calculation for Evaluating Electron Interactions in Mixed Valence Magnetic Systems: Study of 2e-Reduced Lindqvist Polyoxometalates

Nicolas Suaud,*[,†] Xavier López,[‡] Nadia Ben Amor,[†] Nuno A. G. Bandeira,[‡,∥] Coen de Graaf,*[,‡,§] and Josep M. Poblet[‡]

[†]CNRS, Université de Toulouse - UPS, LCPQ-IRSAMC, 118, rte de Narbonne, F-31062 Toulouse Cedex, France

[‡]Departament de Química Física i Inorgànica, Universitat Rovira i Virgili, Marcel·li Domingo s/n, 43007 Tarragona, Tarragona, Spain

[§]Institució Catalana de Recerca i Estudis Avançats (ICREA), Passeig Lluís Companys 23, 08010 Barcelona, Barcelona, Spain

Supporting Information

ABSTRACT: Accurate quantum chemical calculations on real-world magnetic systems are challenging, the inclusion of electron correlation being the bottleneck of such task. One method proposed to overcome this difficulty is the embedded fragment approach. It tackles a chemical problem by dividing it into small fragments, which are treated in a highly accurate way, surrounded by an embedding included at an approximate level. For the vast family of medium-to-large sized polyoxometalates, two-electron-reduced systems are habitual and their magnetic properties are interesting. In this paper, we aim at assessing the quality of embedded fragment calculations by checking their ability to reproduce the electronic spectra of a complete system, here the mixed-metal series $[Mo_xW_{6-x}O_{19}]^{4-}$ (x = 0–6). The microscopic parameters extracted from fragment calculations (electron hopping, intersite electrostatic repulsion, local orbital energy, etc.) have been used to reproduce the spectra through model Hamiltonian calculations. These energies are compared to the results of the highly accurate *ab initio* difference dedicated configuration interaction (DDCI) method on the complete system. In general, the model Hamiltonian calculations using parameters extracted from embedded fragments nearly exactly reproduce the DDCI spectra. This is quite an important result since it can be generalized to any inorganic magnetic system. Finally, the occurrence of singlet or triplet ground states in the series of molecules studied is rationalized upon the interplay of the parameters extracted.

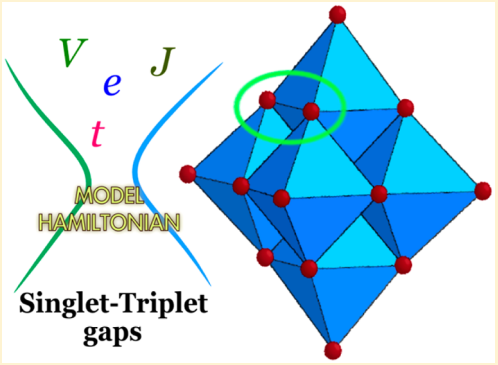

INTRODUCTION

Many strongly correlated systems exhibit quantum properties such as molecular magnetism,[1] colossal magnetoresistance,[2] superconductivity[3] or ferroelectricity,[4] that are of the highest interest for technological applications: data and electrical storage, electron transport, spintronics, etc.[5] These properties are a consequence of complex electronic structures, which require precise quantum chemical methods to be correctly modeled. The difference dedicated configuration interaction (DDCI)[6,7] is one of the most accurate methods for reproducing such properties in this kind of systems. It has been successfully applied to half-filled or mixed-valence systems with one or more unpaired electrons per metal center: cuprates,[8−13] vanadates,[14−17] nickelates,[18,19] manganites,[20,21] cobalt oxides,[22−24] ruthenium complexes,[25] and polyoxometalates (POMs).[26−29] The computational cost of DDCI restricts its use to systems with roughly 50 atoms when the number of unpaired electrons is small (maximum around 5) and even less atoms for systems with more unpaired electrons. An important saving in the computational burden can be obtained by using localized molecular orbitals (MO).[30] Indeed, the size of the CI matrix can be significantly reduced by only considering the interaction between orbitals localized in the same spatial region, as done with the EXSCI method.[31−33] This mainly permits us to treat larger systems with bulkier ligands, although increasing the number of unpaired electrons remains problematic and hence this method is still limited to a small number of magnetic centers.

The embedded fragment method is an elegant way to overcome this bottleneck. It has long been used but mostly restricted to evaluate the hopping and magnetic coupling parameters t and J. In some cases, the accuracy of these values could be assessed by comparing to experimental data, mainly J in half-filled systems. Studies estimating other parameters are less frequent, and direct validity checking of the extracted parameters has solely been based on the comparison of the results of fragments of increasing size. In some cases, indirect checks were done by comparison with experimental data. Instead of processing the whole system at once, the embedded

Received: November 7, 2014
Published: January 7, 2015

DOI: 10.1021/ct5010005
J. Chem. Theory Comput. 2015, 11, 550−559

fragment method makes an accurate evaluation of the interaction between magnetic centers concentrating on a smaller part of the structure. Typically, two interacting centers are selected and a fragment is built by adding the bridging ligand(s) and the first coordination sphere of the metal ion (Figure 1). The structure of the fragment is either extracted

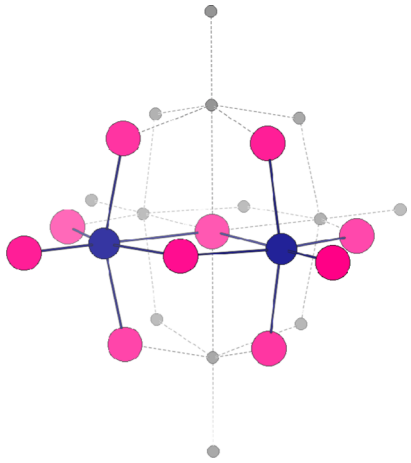

Figure 1. Embedded fragment model to study the interaction between electrons on two metal centers. Colored atoms constitute the *fragment*, and the light-gray region is the *embedding*.

from experimental data (X-ray structures) or from the geometry optimization of the whole system with a density functional theory (DFT) calculation. The isolated fragment does not warrant a correct description of the physics, and, therefore, the main effects of the rest of the molecule/crystal have to be taken into account. This is done by means of an embedding. A simple yet efficient scheme consists in modeling the electric field by point charges and the short-range Coulomb and exchange interactions of the fragment electrons with the nearby centers with effective potentials[34,35] situated at the positions of the ions of the embedding. Other strategies generate a frozen density embedding[36] from the one-electron density obtained in a preceding DFT calculation of the whole system. It should be stressed that adding the embedding does not affect the computational time; all the computational effort can be devoted to the fragment, allowing the use of accurate methods and relatively large atomic basis sets.

A crucial question that has to be addressed concerns the accuracy of the interactions extracted from embedded fragments and how they can reproduce experimental observations or accurate *reference* calculations. Are these interactions transferable to model the physics of the complete system? How important is the role of the embedding and how accurate is its representation with point charges[37] and potentials? These questions have been answered by confronting the fragment results to periodic calculations[38,39] or, more often, by introducing them in a model Hamiltonian (MH) that provides observable macroscopic properties that can be compared to experimental data such as absorption spectra, magnetic susceptibility curves, local spin density, and others.[40,41] It has also been done by comparing the results obtained from fragments of different size.[26] In this case one can directly establish the transferability; if the values of the interactions are similar in both fragments, the effects of the atoms that are in the fragment or in the embedding depending on the size of the fragment are correctly modeled by Total Ion Potentials (TIPs) and charges. It is then possible to argue that the whole embedding fulfills its role.

POMs attract attention in fields as different as medicine, (photo)catalysis, green chemistry, and spintronics. They are 0D systems containing up to a few hundred metal centers.[42] Most of them can accommodate a large number of extra electrons, while keeping their structure almost intact. This leads to versatile mixed-valence magnetic systems in which the extra electrons delocalize over the whole framework. In this article, we focus on Lindqvist POM structures with two extra unpaired electrons (2e) with respect to the natural form, namely $[Mo_6O_{19}]^{4-}$ and $[Mo_5WO_{19}]^{4-}$ (in short 2e-Mo_6 and 2e-Mo_5W, respectively). Although such 2e-reduced forms are thermodynamically unstable, they are excellent models to analyze the accuracy of the embedded fragment model since, contrarily to larger POMs, their moderate size allows a DDCI treatment of the whole molecule that can be used as reference. Figure 2 shows different pictorial representations of the Lindqvist architecture considered here consisting of an octahedral arrangement of six MO_6 units connected by edges, with M = Mo or W. Derivatives containing V, Nb, Ti, and other early transition metal atoms have also been reported. In fully oxidized form, Lindqvist anions contain W^{VI} and Mo^{VI} free of valence metal electrons (d^0 electronic configurations for all M). When it is reduced —electrochemically or by some redox process implying another species— the *extra* electrons are formally occupying molecular orbitals that are combinations of metallic d atomic orbitals (including their delocalization tails on the *oxo* ligands). The most important parameters are the local

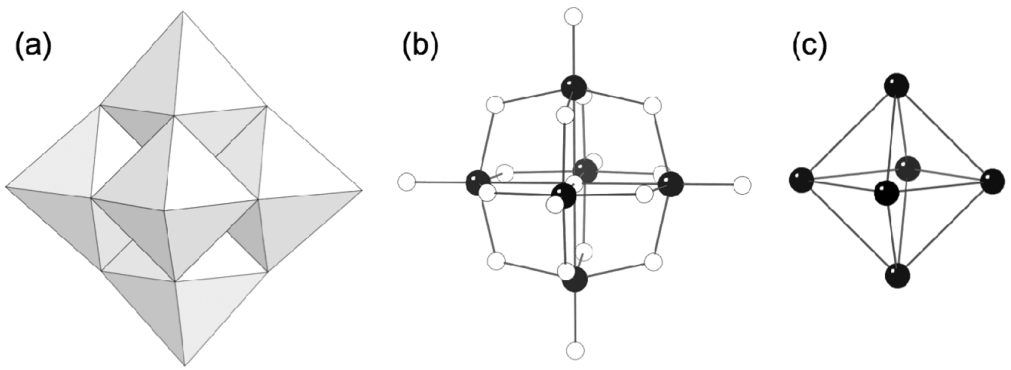

Figure 2. M_6O_{19} Lindqvist structure in (a) polyhedral and (b) ball and stick views. Image (c) corresponds to the M_6 metal cluster only, without oxygens, where lines connecting atoms do not symbolize chemical bonding.

DOI: 10.1021/ct5010005
J. Chem. Theory Comput. 2015, 11, 550−559

orbital energy ε, the hopping integral t, and the interactions between the extra electrons, namely, the magnetic coupling J, the exchange transfer e exemplified in Figure 3, and the intersite

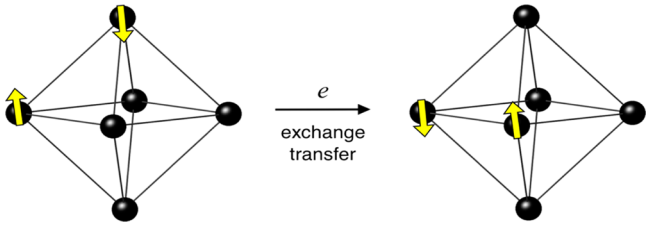

Figure 3. Schematic representation of the exchange transfer e.

electrostatic repulsion V (in fact the difference between the electrostatic repulsion of 2 electrons on nearest versus most separated metal centers). The corresponding model Hamiltonian is given in the Supporting Information (Figure S1).

Theoretical Background and Computational Details. The 2e-reduced structures analyzed in this work were fully optimized at the DFT level using the ADF program.[43−45] We considered the lowest M_S = 1 solution using the unrestricted formalism. The ideal maximal symmetry of the different architectures, O_h (M_6) and C_{4v} (M_5M'), was used. We applied the BP86 functional[46] with triple-ζ + polarization Slater-type atomic basis sets for all atoms and the frozen core approximation for the internal electrons of W (1s-4d), Mo (1s-3d), and O (1s). We applied scalar relativistic corrections to the core electrons by means of the *zeroth-order regular approximation* (ZORA)[47] with the core potentials generated using the DIRAC program.[43] To mimic the external stabilizing effects in solution we introduced the solvent effects of water via the *conductor-like screening model* (COSMO).[48]

For both the complete molecule and the fragment DDCI calculations, 3s3p2d Hay-Wadt type atomic basis sets were used for Mo and W atoms, and all but 14 electrons are modeled by an ECP. For O, a 3s2p atomic basis set is used.[49] As already reported in ref 39, the value of the charges of the embedding is important. It has been shown that formal charges for M═O cationic molecular entities are too large and have to be reduced. A correct modeling of the electrostatic effect MoO^{4+} or WO^{4+} entities is achieved by assigning a +5 charge to Mo(VI) and W(VI) centers and −1 to terminal O(-II). For bridging O(-II), the formal charges have to be used. TIPs for O are taken from MgO.[50] No Mo(VI) or W(VI) TIPs are available, but their ionic radius is similar to that of Ga(III), around 65 pm. Then, Ga TIPs extracted from the K_2NaGaF_6 material are used.[51]

Dynamical polarization and correlation effects are incorporated using the DDCI method implemented in the CASDI code.[52] Since the DDCI method relies on the calculation of different states that share similar spatial descriptions, one has to determine a common set of MOs first and then build the CI space. These orbitals are provided by diagonalizing the CAS +DDCI2 average density matrices of the 15 singlet and 15 triplet states that can be formed by distributing the 2 extra electrons over the 6 metal centers, excluding the states where the 2 electrons are mainly on the same metal. For technical reasons it is not possible to handle the actual point group symmetry of these POMs and calculations are performed in D_{2h} (Mo_6) and C_{2v} (Mo_5W). Nevertheless, the averaging procedure ensures that the molecular orbitals have the symmetry characteristics of the higher point group. An equivalent selection criterion is used for dimer fragments: the singlet ground state and lowest triplet state for calculations with two extra electrons; and the two lowest doublet states for calculations with one extra electron. In the tetramer fragments, we have averaged over the six lowest singlet and six lowest triplet states for calculations with two extra electrons; and the four lowest doublet states for calculations with only one extra electron. Once a common set of orbitals was obtained, CAS +DDCI calculations are performed for the same states.

With the DDCI energies and wave functions at hand, the effective Hamiltonian procedure is used to extract the values of the interactions of the extra electrons. This procedure is extensively described in other articles (see refs 53 and 54 and references therein) and will only be shortly reviewed here. A model space has to be defined: for calculations on the whole POM, the model space contains all the "non-ionic" determinants that can be formed by distributing two electrons on the six metal centers under the restrictions of at most one electron per center; for dimer calculations with one (respectively two) extra electron(s), it consists of the two determinants $|a\rangle$ and $|b\rangle$ (respectively $|a\bar{b}\rangle$ and $|b\bar{a}\rangle$ where a and b are the local magnetic orbitals of each metal center. Then, the elements of the effective Hamiltonian matrix are determined so that its eigenvalues coincide exactly with the DDCI energies of the states (30 states for whole POM calculation, and so on) and its eigenvectors are the projection of the DDCI wave functions onto the model space.

The effective Hamiltonian matrix gives direct access to the value of the microscopic interactions of the extra electrons: the electron transfer t between orbitals a and b is the matrix element between $|a\rangle$and $|b\rangle$ (or $|ac\rangle$ and $|bc\rangle$ for calculations with two extra electrons); the magnetic exchange J is equal to the matrix element between $|a\bar{b}\rangle$ and $|b\bar{a}\rangle$; the electrostatic repulsion between sites A and B is the energy of $|a\bar{b}\rangle$; the orbital energy difference ε between a and b is the difference between the energy of $|a\rangle$ and that of $|b\rangle$; the exchange transfer e is the matrix element between $|a\bar{b}\rangle$ and $|b\bar{c}\rangle$. Instead of working with the absolute value of the electrostatic repulsion, we define V as the energy difference of two determinants with the electrons localized on neighboring or more distant centers. This relative repulsion parameter takes into account all the physics due to electrostatic repulsion effects of the two extra electrons.

The diagonalization of the model Hamiltonians has been done with the MVPACK program[55] or version 9 of Mathematica.

RESULTS AND DISCUSSION

In nearly all studies that use embedded fragment calculations to determine the interactions, attention was only focused on the evaluation of t and J. The extraction of V and ε in POMs done by one of us deserves further analysis because of the approximate character of the extraction procedure.[28] Furthermore, the exchange transfer parameter e is neglected in most of the models of mixed valence systems, whereas it is roughly of the order of J[56,57] and has only been calculated in very few cases. The electronic structure is differently affected by each parameter and has to be emphasized: ε tends to localize the extra electrons on the most oxidant centers (for chemical or structural reasons), whereas t plays the same role as β in the well-known Hückel method and promotes electron delocalization. V tends to separate electrons and either reinforces the action of ε (*trans*-Mo_2W_4 structure, Figure S2c) or acts in

DOI: 10.1021/ct5010005
J. Chem. Theory Comput. 2015, 11, 550−559

Table 1. Comparison of the Values Obtained for the Microscopic Interactions in $Mo_6O_{19}^{4-}$ (meV) for Fragments of Different Size[a]

	t	t'	J	J'	e	e'	V
dimer, 1e/2e	361	−4	−75	0			
tetramer, 1e	381	−120					
tetramer, 2e	358	−121	−46	−5	−41	17	702
full system, 1e	387	−132					
full system, 2e	371/344	−136	−60	−9	−45/−60	21	655

[a] J and J' are nearest and next-nearest neighbor magnetic coupling parameters (negative J indicates antiferromagnetic coupling), t is the hopping integral, and e parametrizes the singlet displacement process. Two values appear for t and e in full system calculations, depending on the relative position of the two electrons. See Figures S3 and S4 for details.

opposition to it (*cis*-Mo_2W_4 form, Figure S2d). The J —usually antiferromagnetic— and e parameters favor the singlet with respect to triplet states, especially when the extra electrons are localized on close metal centers. Hence, it is obvious that the energy and nature (spin multiplicity, electron distribution) of the lowest states and thus the magnetic properties of reduced POMs (and of any mixed valence compound) are determined by a complex interplay of all these parameters and are very sensitive to their value. It is then required to calculate them accurately for evaluating and understanding the properties of such systems.

Since in the vast majority of chemically interesting cases the compounds are too large to be fully treated by accurate computational methods, it is important to provide a strong grounding of the accuracy of embedded fragment evaluations of these parameters. We focus on the magnetic properties of the aforementioned 2e-reduced systems and calculate the low-energy electronic spectra (i.e., all singlet and triplet states formed by distributing two electrons over six centers, excluding double occupancy of any center) to assess the quality of the parameters extracted. The energy levels are directly obtained in the calculations on the complete POM, while the embedded fragment calculations give access to the microscopic parameters listed above that are used in the model Hamiltonian. In addition to discussing the energy spectra, we also tentatively explain the nature of the lowest spin states of the $[Mo_xW_{6-x}O_{19}]^{4-}$ POMs (with x = 0−6, Figure S2), at the end of this article.

This series of Lindqvist POMs has been chosen because their moderate size makes DDCI calculations on the full molecule feasible and thus the subsequent extraction of the effective parameters described above. In a second step, these parameters can be obtained also at the DDCI level but from fragment calculations and then be compared with the former. As the same computational method, basis sets (for the atoms of the whole Lindqvist or fragment) and atom positions are used for a given POM; the comparison of the results gives a direct evaluation of the accuracy of the embedded fragment approach.

$[Mo_6O_{19}]^{4-}$. Let us start by examining the microscopic parameters extracted (Table 1) for the most symmetrical 2e-reduced $Mo_6O_{19}^{4-}$ system (Figure S2a). We have used different fragment approaches, namely dimers (Mo_2O_{10} for nearest-neighbors metal centers and Mo_2O_{11} for farthest metal centers) and a tetramer (Mo_4O_{17}, the 4 Mo atoms forming a square). The results are compared to the *reference* values, extracted from the full system ($Mo_6O_{19}^{4-}$) with the same methodology. In all cases, the 1e- and the 2e-reduced systems are considered to check the stability of the extracted parameters, ideally the hopping integrals should not be dependent on the number of unpaired electrons. Obviously, the bielectronic parameters J, e, and V vanish for the 1e cases. The similar values obtained for the reference and the fragment calculations in Table 1 suggest that the size of the fragment only affects residually the parameters. It can also be seen that t and V clearly dominate over the others, and, consequently, the electronic structure of the ground state is mainly a compromise between these two mechanisms inducing two highly delocalized electrons that are as far as possible from each other. Antiferromagnetic exchange plays only a minor role in the magnetic properties of the system.

The reader can also observe that t' and J' (interactions between most separated metal centers) are smaller when extracted from a dimer than in the full system. The central O^{2-} ion that mediates these interactions is linked to the six metal centers, but four of them are in the embedding, which apparently affects the description of the interaction between metals on opposite sites of the complex. For the same reason, but to a smaller extent, these two parameters are not so well calculated from the tetramer (two Mo atoms are in the embedding). Similarly, V is 7% larger when extracted from the tetramer (702 meV) than from the full molecule (655 meV), evidence of a slight lack of shielding. Even if the physical mechanisms acting are different than for electron hopping or magnetic coupling, we can reasonably assume that this incorrect treatment is also a consequence of a poor description of two of the nearest-neighbors of the central O^{2-} ion. On the contrary, fragment calculations do allow highly accurate evaluations of t and J between nearest metal centers, since all the nearest neighbors of the bridging O^{2-} ion between the two metal centers are inside the fragment. These observations point out the *importance of the shape* of the fragment. Preferably all the atoms that connect the metal centers involved in the interaction should have the full coordination inside the cluster. This may seem a major problem, since all six metals centers should be in the cluster to evaluate t', J', and V. However, a six-coordinated bridging oxygen is only present in the Lindqvist POM. In any other POM the bridging oxygens have a 2- or 3-fold coordination, and DDCI calculations on fragments with three and four metal centers can be done in an almost routine-like fashion, and even five-metal fragments are affordable.

Table 1 also shows that the exchange transfer parameters e and e' are almost identical when extracted from the tetramer (−41 and +17 meV) or from the whole molecule (−45 and +21 meV). e is on the same order of magnitude as J, as expected from the ratio of J/e = 2 derived from a perturbative analysis of the Hubbard model.[56] The positive value of e' (whose perturbative estimate equals $-t{\cdot}t'/U$) is a consequence of the opposite sign of t and t'. Finally, we can see that the hopping parameter t is very similar when extracted from 1e- or 2e-reduced systems. The same is observed for t', although t and t'

DOI: 10.1021/ct5010005
J. Chem. Theory Comput. 2015, 11, 550−559

Table 2. Impact of the Interactions on the Energy Levels (in meV) of $[Mo_6O_{19}]^{4-}$ Obtained with MH Calculations[a]

	^1A_g	^1E_g	^1T_u	^1T_g	^1E_g	^1T_u	^1A_g	^3T_u	^3A_g	^3T_u	^3T_g	^3E_g	^3T_u
DDCI	**0**	187	937	1238	1584	1732	2983	**202**	335	769	1177	2416	2706
MH													
all parameters	**0**	192	879	1235	1527	1775	3063	**198**	343	759	1175	2408	2703
$e = e' = 0$	**0**	77	632	1048	1570	2008	3710	**191**	336	752	1168	2401	2696
$+ J = J' = 0$	**0**	95	694	1110	1598	2070	3757	**153**	278	694	1110	2342	2644
+ effective	**0**	167	848	1211	1601	1940	3407	**179**	483	848	1211	2122	2500
t's													
$t = t' = 0$	**345**	203	972	1032	863	552	0	**232**	912	912	912	912	912
$V = 0$	**124**	1537	536	892	152	1432	2909	**327**	0	416	832	2064	2544

[a]The values are compared to the DDCI results.

Table 3. Comparison of the Values Obtained for the Microscopic Interactions (in meV) in $[Mo_5WO_{19}]^{4-}$ for Fragments of Different Size[b]

	t_{MoW}	t_{belt}	$t_{belt\text{-}apex}$	t'	J_{MoW}	J_{belt}	$J_{belt\text{-}apex}$	ε_W[a]	$\varepsilon_{Mo(apex)}$[a]	V
dimer, 1e/2e	381	361	371		−137	−76	−91	1898	−743	
full system, 1e	402	380	358	−132				2136	−803	
full system, 2e	386	361	340	−136	−86	−56	−53	2103	−790	687

[a]Values relative to the Mo(belt) orbital energy. [b]t, J, and ε are measures of the hopping integral, the magnetic coupling, and the orbital energy, respectively. V is a parameter for the electron repulsion.

are opposite in sign and ∼1/3 in magnitude. Hence it arises that hopping of one electron is marginally affected by the presence of the other extra electron.

The next step consists in evaluating the impact of the value of the parameters on the spectrum of $[Mo_6O_{19}]^{4-}$. Table 2 compares the DDCI reference spectrum calculated for the full molecule (first row) to the MH spectra, reported in the next rows for singlet and triplet states for different sets of parameters. The DDCI results show that the system exhibits strong antiferromagnetic coupling between the two extra electrons; the ^1A_g state, taken as the energy reference, is well below the first excited ^3T_u state. This is consistent with experiments on larger 2e-reduced POMs.[58] The large singlet−triplet gap is also reproduced by the MH calculations: they suit perfectly the whole *ab initio* spectrum of the complete molecule when all model parameters are used. The energy gap between the ground singlet and the lowest triplet state is 202 and 198 meV for DDCI and MH calculation, respectively. The energy difference between the ground state and the highest triplet are also in good agreement: 2703 and 2696 meV for DDCI and MH. This confirms that the low energy physics of the 2e-reduced Lindqvist is governed by the interactions we consider in the model Hamiltonian.

Besides these general observations, MH calculations can selectively establish the role of the parameters on the spectrum, providing information that cannot be assessed from the *ab initio* calculations. This analysis is reported in the lower rows of Table 2. If we impose $e = e' = 0$ or even $e = e' = J = J' = 0$ in the MH calculation, we can see that the $^1A_g - {}^3T_u$ gap is only weakly affected. That means that, quite paradoxically, the coupling between the two electrons remains strongly antiferromagnetic even if $J = 0$, which is usually (when AF) the leading interaction to stabilize singlet versus triplet states. Obviously, other energy differences are strongly affected by eliminating the e and J interactions, for instance the gap between the two lowest singlet states. Using effective t and t' values, which absorb the effect of e into them, gives a good description of the energy levels except for those above 2 eV. The last but one row presents the spectrum putting all the hopping parameters t to zero. Although the singlet−triplet gap is nearly identical to the DDCI value, it must be stressed that the analysis of the wave functions shows that the symmetry and the nature are completely different to that of the lowest states in the DDCI calculations. Hence, the coincidence is purely accidental and reveals the importance of the hopping processes. Similarly, the erroneous results obtained by putting V equal to zero (last row of Table 2) demonstrate the prominence of electron repulsion.

The strong stabilization of the singlet state by t and V deserves some clarifications. A physical analysis of the mechanisms that make ferromagnetic and antiferromagnetic contributions to the coupling is provided in the following sections.

$[Mo_5WO_{19}]^{4-}$. Let us now focus on the $[Mo_5WO_{19}]^{4-}$ ion (Figure S2b). Given the lower electronegativity of W, it is expected that the two electrons will delocalize over the five Mo centers. Remarkably, DDCI points to a triplet ^3A ground state, and the first singlet state, ^1A, is found at 78 meV. The most important effective parameters extracted from dimer and full system DDCI calculations can be found in Table 3; indices *MoW*, *belt*, or *belt-apex* indicate t or J interactions between a belt Mo and W, between two belt Mo's and between a belt Mo and the apical one, respectively. t' is the value of the diagonal hopping integral in the belt. Due to the presence of a W center, an extra parameter (ε) is necessary to model the different orbital energies of the two metals. Moreover, the 4 Mo centers of the belt are structurally different than the Mo in the apex position. Hence, we have to consider ε_W and ε_{Mo}, corresponding to the orbital energy of the W and the apex Mo relative to the orbital energy of the belt Mo atoms. Additionally, different V, e, and e' have to be considered depending on the pairs of centers involved. All these parameters appear in the effective Hamiltonian matrix extracted from the DDCI wave functions and energies of the singlet and triplet states. As expected from the structure of the POM, the electrostatic repulsion is almost the same for any pair of close and any pair of distant metal centers. Then, only the difference of electrostatic repulsion inside the belt is reported.

DOI: 10.1021/ct5010005
J. Chem. Theory Comput. 2015, 11, 550−559

Table 4. Comparison of the Relative Energies of Singlet and Triplet States of $Mo_5WO_{19}^{4-}$ Obtained at the DDCI Level and with a MH Calculation[a]

	^{1}A	^{1}A	^{1}A	^{1}E	^{1}A	^{1}A	^{1}E	^{1}A	^{1}A	^{1}A	^{1}E	^{1}A
DDCI	78	197	567	597	1104	1387	1520	2182	2270	3255	3462	4414
MH	61	259	646	646	1093	1561	1618	2205	2398	3295	3702	4476
	^{3}A	^{3}E	^{3}E	^{3}A	^{3}A	^{3}A	^{3}E	^{3}A	^{3}A	^{3}E	^{3}A	
DDCI	0	218	585	1044	1309	1784	2032	2549	3481	3847	4715	
MH	0	297	619	1132	1387	1818	2084	2629	3562	3953	4818	

[a]A simplified set of parameters is used that does not distinguish the metal centers in intersite interactions: t, t', ε, ε', V, J, and J' are 360, −136, −70, 22, 687, −53, and −9, respectively. ε_W = 2100; $\varepsilon_{Mo(ap)}$ = −800. All values are in meV.

The principal parameters are again well reproduced when they are extracted from calculations on a dimer fragment, notably the three different t's: Mo−W, Mo−Mo in the belt, and Mo(belt)−Mo(apical). All three hopping parameters are of the same order of magnitude. ε is also qualitatively well reproduced with the simplest fragment. This is to our knowledge the first time that the accuracy of such an evaluation is checked. Most interestingly, ε is very positive for W, around 2 eV, and the apical Mo has a surprisingly low ε value. Then, the probability of finding W^V in this system is very low, the extra electrons preferring to occupy the Mo positions, notably the apical one to form Mo^V_{apex}. Given that Mo^{IV}_{apex} is not expected if four Mo_{belt} are still in oxidation state VI, the Mo_5W system features one electron localized in the apical Mo and one electron delocalized over the four belt Mo atoms. Table 3 also shows that V, t, and J are nearly the same as in the Mo_6 complex, and it can be concluded that these parameters are not strongly dependent on the metal nature. The larger ionic radius of W causes the parameters related with electron hopping (t and J) to be somewhat larger and more efficient when W is involved.

The performance of the model parameters can be deduced from Table 4, which reports the DDCI and MH spectra of $[Mo_5WO_{19}]^{4-}$. The latter has been obtained using a set of 9 microscopic parameters, grouping similar parameters into one as specified in the footnote of Table 4. This is more instructive than using the whole set of 24 parameters and permits us to link the macroscopic parameters with the properties of the system. Both DDCI and MH calculations lead to the same triplet ground state. The MH predicts the first singlet 61 meV above in energy, which is slightly smaller than the *exact* 78 meV obtained from DDCI. This difference is due to the simplified set of parameters, since a nearly exact agreement for the triplet-to-lowest-singlet energy gap (80 meV) is obtained diagonalizing the MH with the full set of parameters.

The ferromagnetic coupling in 2e-reduced Mo_5W is very surprising as almost all reduced POMs present strong antiferromagnetic couplings; there are very few examples of paramagnetic[59,60] or ferromagnetic[61,62] POMs. To ensure that the calculated ferromagnetic nature of Mo_5W is not an artifact caused by the geometry optimization of the M_S = 1 state, we repeated the calculations with the M_S = 0 closed-shell optimized geometry. In the M_S = 1 case, one of the extra electrons localizes on the apical Mo ion. This favors a longer $Mo{=}O_{terminal}$ bond and could in principle lead to an artificially low ε for this metal center. This localization is absent in the M_S = 0 determinant. However, the results with the M_S = 0 geometry are practically the same as for the M_S = 1 geometry: $\varepsilon_{Mo(ap)}$ = −790 meV and $t_{belt\text{-}apex}$ = 363 meV, to be compared with −743 and 371 meV from Table 3. The M_S = 0 geometry also leads to a triplet ground state with a similar singlet−triplet gap.

To rationalize the occurrence of a triplet ground state, we analyzed the role of the dominant ε, V, and t parameters. The large positive value of ε_W permits us to exclude the determinants where an electron occupies the W site from the analysis. The remaining determinants can be divided into three groups, schematically represented in Figure 4. The determinants of type (a) are energetically favored by the low orbital energy of the apex Mo ion, while the electrons in the determinants of type (b) are more separated. The relative value of ε and V puts determinants (a) slightly lower in energy, and, hence, we take these as reference. Determinants (b) lie at $(-V-\varepsilon)$ = 103 meV and determinants (c) have an energy of $-\varepsilon$ = 790 meV with respect to determinants (a).

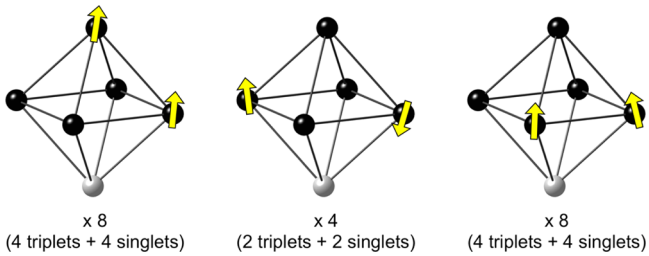

Figure 4. Most probable distributions of two electrons in Mo_5W (Mo: black, W: gray). The determinants are grouped in three families of increasing energy: (a) 1e in Mo_{apex} and 1e in $(Mo_{belt})_4$, (b) 2e in $(Mo_{belt})_4$ in next nearest neighbors, (c) 2e in $(Mo_{belt})_4$ in nearest neighbors.

To identify the mechanisms that contribute most to the triplet ground state of the Mo_5W complex, we have constructed model Hamiltonians with t_{belt}, $t_{belt\text{-}ap}$, t', ε, and V in different model spaces spanned by determinants of a, b, c, (a+b), (a+c), and (a+b+c). The resulting energy levels are shown in Figure 6. Diagonalization of the simplest model spaces (determinants a, b, or c) does not lift the degeneracy of singlet and triplet states. The lowest states are formed by a linear combination of (a) determinants under the action of the hopping parameter t_{belt} and have one electron localized on Mo_{apex} and the other delocalized over the belt. This shows that the hopping of one electron over the belt is not enough to create a singlet−triplet gap. The introduction of the interaction of determinants (a) and (b) in model space (a+b) leads to an important stabilization of the singlet state, while the corresponding triplet is not affected. The electrons circulate in two triangles under the action of a positive $t_{belt\text{-}apex}$ and a negative t' (see Figure 5, left). As shown in Figure S5, the circular movement of two electrons on a triangle with two positive and one negative hopping parameter always leads to a singlet state and explains the antiferromagnetic contribution of the interaction of the (a) and (b) spaces. The interaction introduces a slight delocaliza-

DOI: 10.1021/ct5010005
J. Chem. Theory Comput. 2015, 11, 550−559

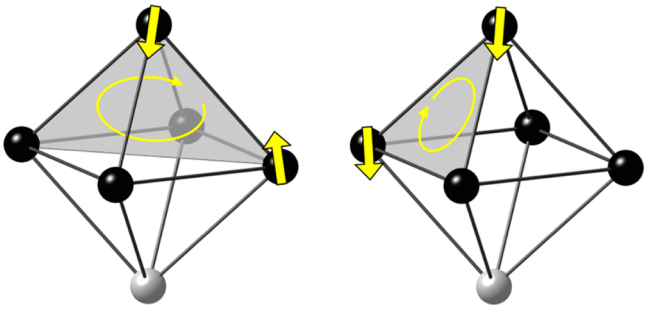

Figure 5. Schematic representation of the circular movement of the two electrons due to t' and $t_{belt\text{-}apex}$ (left) and and t_{belt} and $t_{belt\text{-}apex}$ (right). The light sphere represent W, the darker ones Mo.

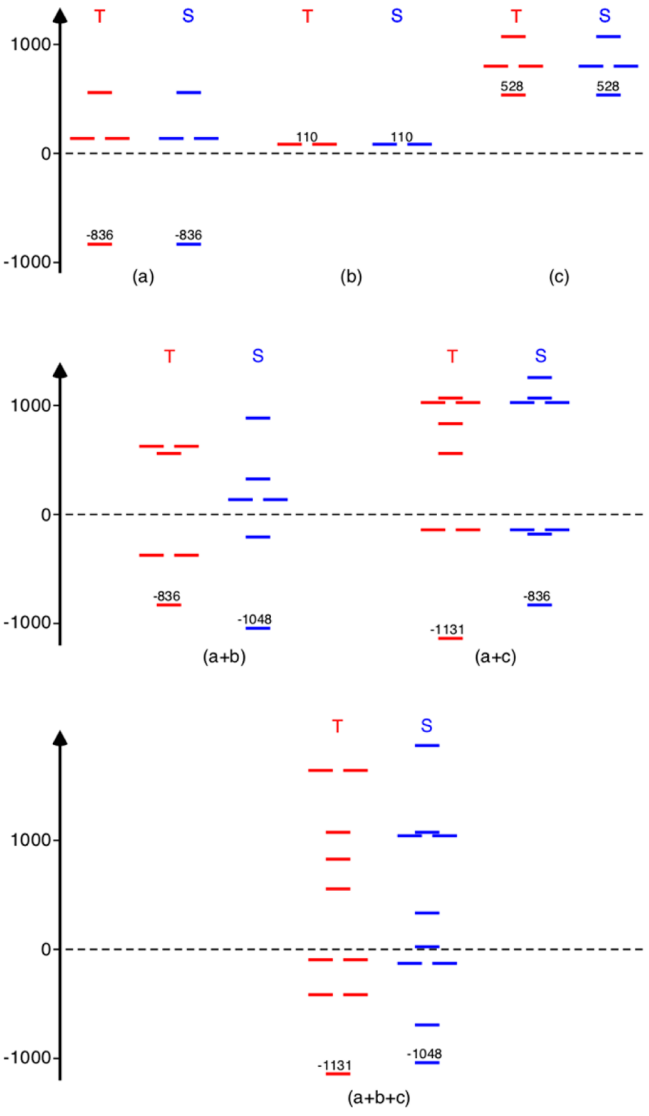

Figure 6. Energy diagrams for Mo_5W showing the triplet (red) and singlet (blue) states arising from each family of determinants. The final spectrum (a+b+c) is comparable to the values in Table 4, with a triplet ground state. The vertical scales are in meV units.

tion of the electron on Mo_{apex} over the belt. However, the wave function remains strongly dominated by the type (a) determinants.

The interaction of (a) and (c) in the (a+c) model space provides a strong stabilization of the lowest triplet by approximately 300 meV. Again, the interaction of (a) with (c) introduces a circulation of electrons on a triangle (four in this case, see Figure 5 right), but now the hopping parameters involved (t_{belt} and $t_{belt\text{-}apex}$) are positive and referring to Figure S6, this mechanism supports a triplet ground state. The diagonalization of the (a+b+c) model space does not introduce any new stabilization of the lowest triplet and singlet states; the final ground state has triplet spin coupling and a gap of 83 meV with the singlet, in good agreement with the DDCI calculation on the whole molecule. Hence, it can be concluded that despite being higher in energy, the determinants of type (c) play a key role in the ferromagnetic ground state of the Mo_5W complex. Their dominance over the antiferromagnetic effect introduced by the lower-lying (b) determinants can be ascribed to (i) the fact that the Mo_5W complex has four triangles where the ferromagnetic mechanism is active and only two with an antiferromagnetic contribution, and (ii) the relative values of t and t' ($|t| > |t'|$). The antiferromagnetic mechanism involves t and t', whereas the ferromagnetic contribution involves t only.

An essential factor for the ferromagnetic nature of the complex is the localization of one of the electrons on the apical Mo ion due to the very negative value of $\varepsilon_{Mo(ap)}$. By gradually increasing this value, the weight of the (a)-type determinants in the wave function decreases, which is accompanied by a closure of the triplet-singlet gap. At $\varepsilon_{Mo(ap)} \approx -400$ meV, the singlet becomes the most stable state.

$[Mo_4W_2O_{19}]^{4-}$ to $[MoW_5O_{19}]^{4-}$. Considering that model Hamiltonians are capable of reproducing the antiferromagnetic character of Mo_6 and the ferromagnetic ground state of Mo_5W, we conclude that the parameter extraction based on embedded dimers is sufficiently accurate. Moreover, the observation that the parameters extracted for Mo_6 and Mo_5W are similar suggests that they are transferable from one system to another. Therefore, we now analyze the nature of the ground state for the rest of the family (Mo_4W_2 to MoW_5, Figure S2c–i) using the parameters listed in Tables 2 and 3. The singlet–triplet splitting is determined by diagonalization of the corresponding model Hamiltonian for each member of the series, and the results are compared to the Mo_6 and Mo_5W values in Table 5.

Because of the high W orbital energy, the two electrons in *trans*-Mo_4W_2 are effectively confined to the square formed by the four equatorial Mo ions. The large singlet stability in this molecule —in fact comparable to what is found for Mo_6— is easily rationalized by considering the effect of the nearest-neighbors hopping t and the repulsion V. The lowest-lying determinants can be divided into two groups. The first group consists of four determinants with the two electrons on the diagonal of the square. They form two singlets and two triplets, which are degenerate in the present t-V model. The determinants of the second group have the two electrons on neighboring centers and lie at an energy V with respect to the singlets and triplets of group 1. The two types of determinants interact via t, and a second order perturbative evaluation of the t-V model Hamiltonian (see Figure S7) shows that the two triplet states are stabilized by $4t^2/V$, while one of the singlet states is lowered by $8t^2/V$. This strongly resembles the contribution of the well-known Anderson mechanism to the stability of the low-spin state in biradical systems for which this contribution reads $4t^2/U$, U being the on-site repulsion, defined as the energy difference between the determinant with two electrons on neighboring sites and the determinant with two electrons localized on the same center. Since V is significantly smaller than U, the stabilization of the singlet in Mo_4W_2 is

DOI: 10.1021/ct5010005
J. Chem. Theory Comput. 2015, 11, 550–559

Table 5. Energy Difference (in meV) between the Lowest Singlet and Triplet States[a] Predicted from MH Calculations with the Parameters Extracted from Mo_6 and Mo_5W Compounds

			Mo_4W_2		Mo_3W_3		Mo_2W_4			
	Mo_6	Mo_5W	*cis*	*trans*	*mer*	*fac*	*cis*	*trans*	MoW_5	W_6
MH	−198	61	−155	−193	−49	352	6	12	−29	−238

[a]Negative values indicate a singlet ground state.

considerable. It is more complicated to give an explanation of the stability of the singlet in the *cis*-Mo_4W_2 complex. ε favors the localization of the electrons on the Mo diametrically opposed to the W centers (Mo_{opp}), whereas V favors the localization on the two other centers. The former determinants are lower by about $-2\varepsilon + V \approx 900$ meV compared to the latter ones and $-\varepsilon + V \approx 200$ meV lower compared to determinants with only one occupied Mo_{opp}. A perturbative decomposition shows that the third order contribution to the coupling (that only involves t hopping integrals) is antiferromagnetic (≈−290 meV), whereas the fourth order contribution (involving one t' integral) is ferromagnetic (≈100 meV). The net effect of these two contributions results in a singlet stability, in agreement with the value of Table 5.

The *mer*- and *fac*-isomers of Mo_3W_3 show opposite spin stability. The former has a singlet ground state, whereas the latter shows triplet coupling. The origin of this difference lies in the topology of the two isomers. In the *fac*-isomer, the three Mo ions that share the two extra electrons lie on a face-triangle of the complex, activating the triplet stabilization found in Mo_5W. Since the three Mo ions are equivalent, this circulation is not hindered by the localization of an electron on one of the centers as in Mo_5W and therefore more effective leading to a larger triplet-singlet gap. On the other hand, the hopping processes in the Mo_3 triangle of the *mer*-isomer involve two positive and one negative t, leading to a singlet ground state.

The *cis* and *trans* isomers of the Mo_2W_4 system show almost degenerate singlet and triplet states. This is a direct consequence of the high degree of localization of the electrons on the two Mo centers. The large value of ε_W nearly completely deactivates electron hopping and leads to very weakly interacting electrons. The electronic structure of the MoW_5 complex is also dominated by two highly localized electrons. One electron naturally localizes on the Mo center, while the second one is basically confined to the W center on the opposite end of the complex due to the electron repulsion V. Finally, we observe a strong singlet stabilization in W_6. This complex is practically equivalent to the Mo_6 system, albeit the hopping parameter among the W atoms is larger than for Mo (440 meV instead of 371 meV), leading to a somewhat larger singlet−triplet gap.

CONCLUSIONS

The results described in this paper provide a firm basis for the extraction of a wide range of electronic structure parameters from embedded fragment calculations. The interactions between unpaired electrons in inorganic systems —hopping integral (t), magnetic coupling (J), exchange transfer (e), intersite electrostatic repulsion (V), and local orbital energy (ε)— have been extracted from embedded fragments and compared with the outcomes of the whole system. The values obtained in both approaches are similar. This has important consequences since the interactions considered here appear in most compounds with interesting quantum properties: magnetism, superconductivity, giant or colossal magnetoresistivity, ferroelectricity, etc. and are in general not easily extracted from the complete system.

This work compares results obtained from embedded fragments to the benchmark values obtained by computing the whole system, providing a clear-cut accuracy check of the embedded fragment method. Two Lindqvist POMs, namely $Mo_6O_{19}^{4-}$ and $Mo_5W_6O_{19}^{4-}$, are selected for two reasons. In the first place, DDCI calculations are still feasible on the whole structure and, second, because these complexes exhibit all the interactions listed above. The calculated values are used to parametrize a model Hamiltonian, allowing us to obtain macroscopic properties that can be compared to experimental observations and to address the importance of the different interactions on these macroscopic properties.

Finally, the special character of the electrostatic repulsion V has to be remarked. Contrary to ε, which is local and t, J, and e, which decrease very rapidly with the distance between the metal centers, the electrostatic repulsion is intrinsically long-ranged. Therefore, it has to be evaluated for each pair of metal centers and cannot be determined only from fragments containing nearest or next-nearest neighbor metal centers. Actually, it requires fragments based on all pairs of metal centers and have to consider the shielding effect of all highly polarizable centers, O^{2-}, in the case of POMs. This evaluation is still a challenge for large systems: the simple $1/r$ evaluation of V that has been used up to now in POM studies is too crude (the shielding effects of the *oxo* anions are neglected), giving a value of 1260 meV that is almost twice the DDCI one (650−700 meV); a forthcoming paper will be devoted to this point. Also, in larger POMs, e and J will not play any role in the spectra, then we just have to focus on t, V, and ε. Extracting t is not a problem, and ε is extracted simultaneously.

ASSOCIATED CONTENT

Supporting Information

Figures S1−S7: Explicit form of the model Hamiltonian, graphical representation of the $[Mo_xW_{6-x}O_{19}]^{4-}$ systems, details on t and e, model Hamiltonian for electron circulation on a triangle and a square. This material is available free of charge via the Internet at http://pubs.acs.org.

AUTHOR INFORMATION

Corresponding Authors

*E-mail: suaud@irsamc.ups-tlse.fr (N.S.).
*E-mail: coen.degraaf@urv.cat (C.d.G.).

Present Address

[‖]Institut Català d'Investigació Química (ICIQ), Av/Països Catalans 16, 43007 Tarragona, Spain.

Notes

The authors declare no competing financial interest.

DOI: 10.1021/ct5010005
J. Chem. Theory Comput. 2015, 11, 550−559

■ ACKNOWLEDGMENTS

The authors are grateful to COST Action CM1303 "Polyoxometalate Chemistry for Molecular Nanoscience (PoCheMoN)" for supporting this work. This work was granted access to the HPC resources of CALMIP under the allocation 2012-1044. Nicolas Suaud thanks C'Nano for financial support. We are also grateful to the Spanish Government (Projects CTQ2011-23140 and CTQ2011-29054), the Generalitat de Catalunya (Project 2014SGR199), and the Xarxa de Referència en Química Teòrica i Computacional, XRQTC). We are grateful to the MVPACK authors.

■ REFERENCES

(1) (a) Gatteschi, D.; Sessoli, R.; Villain, F. *Molecular Nanomagnets*; Oxford University Press: Oxford, 2006. (b) *Spin-Crossover Materials – Properties and Applications*; Halcrow, M. A., Ed.; Wiley: Chichester, United Kingdom, 2013.
(2) (a) Salamon, M. B.; Jaime, M. *Rev. Mod. Phys.* **2001**, *73*, 583–628. (b) Dagotto, E. *New J. Phys.* **2005**, *7*, 67. (c) Murakami, Y.; Kasai, H.; Kim, J. J.; Mamishin, S.; Shindo, D.; Mori, S.; Tonomura, A. *Nat. Nanotechnol.* **2010**, *5*, 37–41.
(3) (a) Johnston, D. C. *Adv. Phys.* **2010**, *59*, 803–1061. (b) Fausti, D.; Tobey, R. I.; Dean, N.; Kaiser, S.; Dienst, A.; Hoffmann, M. C.; Pyon, S.; Takayama, T.; Takagi, H.; Cavalleri, A. *Science* **2011**, *331*, 189–191.
(4) (a) Spaldin, N. A.; Cheong, S.-W.; Ramesh, R. *Phys. Today* **2010**, *63*, 38–43. (b) Daumont, C. J. M.; Farokhipoor, S.; Ferri, A.; Wojdel, J. C.; Iñiguez, J.; Kooi, B. J.; Noheda, B. *Phys. Rev. B* **2010**, *81*, 144115. (c) Valla, T.; Fedorov, A. V.; Lee, J.; Davis, J. C.; Gu, G. D. *Science* **2006**, *314*, 1914–1916.
(5) (a) Žutić, I.; Fabian, J.; Das Sarma, S. *Rev. Mod. Phys.* **2004**, *76*, 323–410. (b) Bogani, L.; Wernsdorfer, W. *Nat. Mater.* **2008**, *7*, 179–186. (c) Létard, J.-F.; Guionneau, P.; Goux-Capes, L. In *Spin crossover in Transition Metal Compounds III*; Gütlich, P., Goodwin, H. A., Eds.; Springer-Verlag: Berlin, 2004; Vol. *235* of *Top. Curr. Chem.* pp 221–249.
(6) Miralles, J.; Daudey, J.-P.; Caballol, R. *Chem. Phys. Lett.* **1992**, *198*, 555–562.
(7) Miralles, J.; Castell, O.; Caballol, R.; Malrieu, J.-P. *Chem. Phys.* **1993**, *172*, 33–43.
(8) Calzado, C. J.; Sanz, J. F.; Malrieu, J.-P. *J. Chem. Phys.* **2000**, *112*, 5158–5167.
(9) Muñoz, D.; Illas, F.; de P. R. Moreira, I. *Phys. Rev. Lett.* **2000**, *84*, 1579–1582.
(10) de Graaf, C.; Illas, F. *Phys. Rev. B* **2001**, *63*, 014404.
(11) Gellé, A.; Lepetit, M.-B. *Eur. Phys. J. B* **2005**, *43*, 29–37.
(12) Petit, S.; Lepetit, M.-B. *Europhys. Lett.* **2009**, *87*, 67005.
(13) Pradipto, A. M.; Maurice, R.; Guihéry, N.; de Graaf, C.; Broer, R. *Phys. Rev. B* **2012**, *85*, 014409.
(14) Suaud, N.; Lepetit, M.-B. *Phys. Rev. B* **2000**, *62*, 402–409.
(15) Lepetit, M.-B.; Suaud, N. *Int. J. Mod. Phys. B* **2001**, *15*, 1377–1380.
(16) Suaud, N.; Lepetit, M.-B. *Phys. Rev. Lett.* **2002**, *88*, 056405.
(17) Hozoi, L.; Presura, C.; de Graaf, C.; Broer, R. *Phys. Rev. B* **2003**, *67*, 035117.
(18) de P. R. Moreira, I.; Suaud, N.; Guihéry, N.; Malrieu, J.-P.; Caballol, R.; Bofill, J. M.; Illas, F. *Phys. Rev. B* **2002**, *66*, 134430.
(19) Bastardis, R.; Guihéry, N.; de Graaf, C. *Phys. Rev. B* **2007**, *76*, 132412.
(20) Bastardis, R.; Guihéry, N.; Suaud, N.; de Graaf, C. *J. Chem. Phys.* **2006**, *125*, 194708.
(21) Bastardis, R.; Guihéry, N.; Suaud, N. *Phys. Rev. B* **2007**, *75*, 132403.
(22) Soret, J.; Lepetit, M.-B. *Phys. Rev. B* **2012**, *85*, 165145.
(23) Landron, S.; Soret, J.; Lepetit, M.-B. *J. Phys.: Condens. Matter* **2010**, *22*, 345603.
(24) Gellé, A.; Varignon, J.; Lepetit, M.-B. *Europhys. Lett.* **2009**, *88*, 37003.
(25) Bolvin, H. *J. Phys. Chem. A* **2003**, *107*, 5071–5078.
(26) Suaud, N.; Gaita-Ariño, A.; Clemente-Juan, J. M.; Sánchez-Marín, J.; Coronado, E. *J. Am. Chem. Soc.* **2002**, *124*, 15134–15140.
(27) Suaud, N.; Gaita-Ariño, A.; Clemente-Juan, J. M.; Coronado, E. *Chem.—Eur. J.* **2004**, *10*, 4041–4053.
(28) Clemente-Juan, J. M.; Coronado, E.; Gaita-Ariño, A.; Suaud, N. *J. Phys. Chem. A* **2007**, *111*, 9969–9977.
(29) Calzado, C. J.; Clemente-Juan, J. M.; Coronado, E.; Gaita-Ariño, A.; Suaud, N. *Inorg. Chem.* **2008**, *47*, 5889–5901.
(30) Maynau, D.; Evangelisti, S.; Guihéry, N.; Malrieu, J.-P.; Calzado, C. J. *J. Chem. Phys.* **2002**, *116*, 10060–10068.
(31) Bories, B.; Maynau, D.; Bonnet, M.-L. *J. Comput. Chem.* **2007**, *28*, 632–643.
(32) Ben Amor, N.; Bessac, F.; Hoyau, S.; Maynau, D. *J. Chem. Phys.* **2011**, *135*, 014101.
(33) Chang, C.; Calzado, C. J.; Ben Amor, N.; Sánchez-Marín, J.; Maynau, D. *J. Chem. Phys.* **2012**, *137*, 104102.
(34) Winter, N. W.; Pitzer, R. M.; Temple, D. K. *J. Chem. Phys.* **1987**, *86*, 3549–3556.
(35) Barandiarán, Z.; Seijo, L. *J. Chem. Phys.* **1988**, *89*, 5739–5746.
(36) Wesolowski, T. A.; Warshel, A. *J. Phys. Chem.* **1993**, *97*, 8050–8053.
(37) Gellé, A.; Lepetit, M.-B. *J. Chem. Phys.* **2008**, *128*, 244716.
(38) de P. R. Moreira, I.; Illas, F. *Phys. Rev. B* **1997**, *55*, 4129–4137.
(39) Lepetit, M.-B.; Suaud, N.; Gellé, A.; Robert, V. *J. Chem. Phys.* **2003**, *118*, 3966–3973.
(40) Jornet-Somoza, J.; Deumal, M.; Robb, M. A.; Landee, C. P.; Turnbull, M. M.; Feyerherm, R.; Novoa, J. J. *Inorg. Chem.* **2010**, *49*, 1750–1760.
(41) Calzado, C. J. *Chem.—Eur. J.* **2012**, *19*, 1254–1261.
(42) (a) Pope, M. T. *Heteropoly and Isopoly Oxometalates*; Springer: Berlin, 1983. (b) Müller, A.; Roy, S. In *The Chemistry of Nanomaterials: Synthesis, Properties and Applications*; Wiley-VCH: Weinheim, 2004. (c) Long, D.-L.; Tsunashima, R.; Cronin, L. *Angew. Chem., Int. Ed.* **2010**, *49*, 1736–1758;(d) Special issue on polyoxometalate chemistry: *Chem. Soc. Rev.* **2012**, *41*, 7325–7326.
(43) *ADF2009.01*, SCM, Theoretical Chemistry, Vrije Universiteit, Amsterdam, The Netherlands, http://www.scm.com (accessed Dec 20, 2014).
(44) Fonseca Guerra, C.; Snijders, J. G.; Te Velde, G.; Baerends, E. J. *Theor. Chem. Acc.* **1998**, *99*, 391–403.
(45) Te Velde, G.; Bickelhaupt, F. M.; van Gisbergen, S. J. A.; Fonseca Guerra, C.; Baerends, E. J.; Snijders, J. G.; Ziegler, T. *J. Comput. Chem.* **2001**, *22*, 931–967.
(46) (a) Becke, A. D. *Phys. Rev. A* **1988**, *38*, 3098–3100. (b) Vosko, S. H.; Wilk, L.; Nusair, M. *Can. J. Phys.* **1980**, *58*, 1200–1211. (c) Perdew, J. P. *Phys. Rev. B* **1986**, *33*, 8822–8824.
(47) (a) van Lenthe, E.; Ehlers, A. E.; Baerends, E. J. *J. Chem. Phys.* **1999**, *110*, 8943–8953. (b) van Lenthe, E.; Baerends, E. J.; Snijders, J. G. *J. Chem. Phys.* **1993**, *99*, 4597–4610. (c) van Lenthe, E.; Baerends, E. J.; Snijders, J. G. *J. Chem. Phys.* **1994**, *101*, 9783–9792. (d) van Lenthe, E.; Snijders, J. G.; Baerends, E. J. *J. Chem. Phys.* **1994**, *105*, 6505–6516. (e) van Lenthe, E.; van Leeuwen, R.; Baerends, E. J.; Snijders, J. G. *Int. J. Quantum Chem.* **1996**, *57*, 281–293.
(48) (a) Klamt, A.; Schüürmann, G. *J. Chem. Soc., Perkin Trans.* **1993**, *2*, 799–805. (b) Andzelm, J.; Kölmel, C.; Klamt, A. *J. Chem. Phys.* **1995**, *103*, 9312–9320. (c) Klamt, A. *J. Chem. Phys.* **1995**, *99*, 2224–2235. (d) Implemented in the ADF package by Pye, C. C.; Ziegler, T. *Theor. Chem. Acc.* **1999**, *101*, 396–408.
(49) Hay, P. J.; Wadt, W. R. *J. Chem. Phys.* **1985**, *82*, 299–310.
(50) Pascual, J. L.; Seijo, L.; Barandiarán, Z. *J. Chem. Phys.* **1993**, *98*, 9715–9724. Nygren, M. A.; Pettersson, L. G. M.; Barandiarán, Z.; Seijo, L. *J. Chem. Phys.* **1994**, *100*, 2010–2018.
(51) Seijo, L.; Barandiarán, Z.; Pettersson, L. G. M. *J. Chem. Phys.* **1993**, *98*, 4041–4046.
(52) Ben Amor, N.; Maynau, D. *Chem. Phys. Lett.* **1998**, *286*, 211–220.

DOI: 10.1021/ct5010005
J. Chem. Theory Comput. 2015, 11, 550–559

(53) Maurice, R.; de Graaf, C.; Guihéry, N. *Phys. Chem. Chem. Phys.* **2013**, *15*, 18784−18804.
(54) Malrieu, J.-P.; Caballol, R.; Calzado, C. J.; de Graaf, C.; Guihéry, N. *Chem. Rev.* **2014**, *114*, 429−492.
(55) Borrás-Almenar, J. J.; Cardona-Serra, S.; Clemente-Juan, J. M.; Coronado, E.; Palii, A. V.; Tsukerblat, B. S. *J. Comput. Chem.* **2010**, *31*, 1321−1332.
(56) From a second order perturbation expansion in the Hubbard model space, the magnetic exchange between a and b is $J = -^{2t2}_{ab}/U$, while the exchange transfer parameter between $|\rangle$ and $|b\rangle$ $e = -t_{ab}t_{bc}/U$, where t_{ab} and t_{bc} are the hopping parameters between a and b and b and c, respectively. U is the energy of the ionic forms $|a$ and $|b$.
(57) Calzado, C. J.; Malrieu, J.-P. *Phys. Rev. B* **2001**, *63*, 214520.
(58) Casañ-Pastor, N.; Baker, L. C. W. *J. Am. Chem. Soc.* **1992**, *114*, 10384−10394.
(59) Bi, L.-H.; Kortz, U.; Dickman, M. H.; Nellutla, S.; Dalal, N. S.; Nadjo, L.; Prinz, M.; Neumann, M. *J. Cluster Sci.* **2006**, *17*, 143−165.
(60) Suaud, N.; Masaro, Y.; Coronado, E.; Clemente-Juan, J. M.; Guihéry, N. *Eur. J. Inorg. Chem.* **2009**, 5109−5114.
(61) Manos, M. J.; Tasiopoulos, A. J.; Tolis, E. J.; Lalioti, N.; Woollins, J. D.; Slawin, A. M. Z.; Sigalas, M. P.; Kabanos, T. A. *Chem.—Eur. J.* **2003**, *9*, 695−703.
(62) Zueva, E. M.; Borshch, S. A.; Petrova, M. M.; Chermette, H.; Kuznetsov, A. M. *Eur. J. Inorg. Chem.* **2007**, 4317−4325.

DOI: 10.1021/ct5010005
J. Chem. Theory Comput. 2015, 11, 550−559